
Planetary Science: A Lunar Perspective

STUART ROSS TAYLOR

Lunar and Planetary Institute
Houston, Texas, U.S.A.

and
Research School of Earth Sciences
Australian National University
Canberra, Australia

LUNAR AND PLANETARY INSTITUTE
3303 NASA ROAD 1
HOUSTON, TEXAS 77058



Copyright © 1982 by the Lunar and Planetary Institute.

This work relates to NASA Contract No. NASW-3389 with Universities Space Research Association. The U.S. Government has a royalty-free license to exercise all rights under the copyright claimed herein for Governmental purposes. All other rights are reserved by the Lunar and Planetary Institute.

Typeset by the Lunar and Planetary Institute, printed by Publishers Production International, and bound by Arnold's Bindery in the United States of America.

Library of Congress Cataloging in Publication Data available from the Library of Congress CIP Division, or from the publisher.

Cover: An artistic perception of a portion of Mare Ingenii (S. Adlis-Vass, artist).

Back cover: An artistic rendition of the view south across Mare Imbrium (S. Adlis-Vass, artist).

CONTENTS

Preface	i
Acknowledgments	ix
Chapter 1 The Exploration of the Solar System	1
1.1 Early Influences	1
1.2 Lunar Sampling	3
1.3 The Moon and the Solar System	12
References and Notes	15
Chapter 2 Geology and Stratigraphy	17
2.1 The Face of the Moon	17
2.2 Stratigraphy of the Lunar Surface	26
2.3 Radiometric and Stratigraphic Lunar Time Scales	29
2.4 Detailed Lunar Stratigraphy	32
2.4.1 Pre-Imbrian	32
2.4.2 Pre-Nectarian	33
2.4.3 Nectarian	33
2.4.4 The Imbrian System	36
2.4.5 Eratosthenian System	39
2.4.6 Copernican System	39
2.5 Mercury	40
2.5.1 Intercrater Plains	40
2.5.2 The Heavily Cratered Terrain	44
2.5.3 Smooth Plains	47
2.5.4 Lobate Scarps	47
2.6 Mars	50
2.6.1 The Ancient Cratered Terrain	51
2.6.2 Volcanic Plains and Mountains	51
2.7 Venus	55
2.8 Gallilean and Saturnian Satellites	57
References and Notes	57
Chapter 3 Meteorite Impacts, Craters and Multi-Ring Basins	61
3.1 The Great Bombardment	61
3.2 The Volcanic/Meteorite Impact Debate	62
3.3 The Mechanism of Crater Formation	64
3.4 Simple Bowl-Shaped Impact Craters	68
3.5 Large Wall-Terraced Craters, Central Peaks and Peak Rings	71

3.6	The Multi-Ring Basins	76
3.7	Depth of Excavation of Basins	87
3.8	Basin Diameter-Morphology Relationship	91
3.9	Impact Melts and Melt Sheets	92
3.10	Secondary Impact Craters	93
3.11	Dark-Halo Craters	96
3.12	Smooth-Rimmed Craters and Floor-Fractured Craters	97
3.13	Isostatic Compensation of Craters	99
3.14	Linné Crater and Transient Phenomena	100
3.15	Swirls	100
3.16	Meteorite Flux	100
3.17	The Cratering Record and the Lunar Cataclysm	104
3.18	Secondary Cratering and the Cayley Problem	109
	References and Notes	110
Chapter 4 Planetary Surfaces		115
4.1	The Absence of Bedrock	115
4.2	The Extreme Upper Surface	116
4.3	The Regolith	117
4.3.1	Thickness and Mechanical Properties	118
4.3.2	Structure	121
4.3.3	Rate of Accumulation	123
4.3.4	“Ages” of the Soils	123
4.3.5	Soil Breccias and Shock Metamorphism of Lunar Soils	127
4.4	Glasses	128
4.4.1	Agglutinates	128
4.4.2	Impact Glasses	130
4.4.3	Tektites	135
4.5	Chemistry and Petrology of the Regolith	139
4.5.1	Metallic Iron in the Lunar Regolith	142
4.5.2	Volatile Element Transport on the Lunar Surface	147
4.5.3	The Meteoritic Component	151
4.6	Microcraters and Micrometeorites	151
4.7	Irradiation History of the Lunar Surface	155
4.7.1	Solar Wind	155
4.7.2	Solar Flares	155
4.7.3	Galactic Cosmic Rays	157
4.8	Physical Effects of Radiation	157
4.9	Chemical and Isotopic Effects	159
4.9.1	Carbon, Nitrogen and Sulfur	159
4.9.2	The Rare Gases	161

4.9.3	The Argon-40 Anomaly	162
4.9.4	Cosmogenic Radionuclides	163
4.9.5	Thermal Neutron Flux	163
4.10	Exposure Ages and Erosion Rates	163
4.10.1	Nuclear Track Data	165
4.10.2	Rare Gas Data	166
4.11	Solar and Cosmic Ray History	167
4.12	The Lunar Atmosphere	169
4.13	Rare Gases and Planetary Atmospheres	169
4.14	Organic Geochemistry and Exobiology	171
	References and Notes	171
Chapter 5 Planetary Crusts		177
5.1	The Lunar Highland Crust	180
5.1.1	Thickness and Density	180
5.1.2	The Megaregolith	186
5.2	Breccias	187
5.2.1	Monomict Breccias	191
5.2.2	Dimict Breccias	192
5.2.3	Feldspathic Fragmental Breccias	194
5.2.4	Impact Melt Breccias	195
5.2.5	Granulitic Breccias	198
5.2.6	Basalts in Highland Breccias	200
5.3	Melt Rocks	201
5.4	Highland Crustal Components	201
5.4.1	Anorthosites	205
5.4.2	The Mg Suite	206
5.4.3	KREEP	208
5.4.4	KREEP Volcanism in the Lunar Highlands?	214
5.5	Volatile Components in the Highland Crust	216
5.6	The Ancient Meteorite Component	219
5.7	Pristine Rocks in the Lunar Highlands	221
5.8	The Orbital Chemical Data	223
5.9	The Chemical Composition of the Highland Crust	227
5.9.1	Element Correlations	228
5.9.2	Highland Crustal Abundances	230
5.10	Age and Isotopic Characteristics of the Highland Crust	233
5.10.1	The Oldest Ages	233
5.10.2	The 4.2 Aeon Ages	238
5.10.3	Basin Ages and the Lunar Cataclysm	240
5.11	Evolution of the Highland Crust	242
5.11.1	The Magma Ocean	242

5.11.2	How Long did the Early Highland Crust Take to Evolve?	244
5.11.3	Crystallization History of the Lunar Crust	246
5.12	The Crust of the Earth	253
5.13	Other Planetary Crusts	256
	References and Notes	258
Chapter 6	Basaltic Volcanism	263
6.1	Floods of Basaltic Lava	263
6.1.1	Thickness of Mare Fill	265
6.1.2	Age of the Oldest Mare Surface	266
6.1.3	The Lunar Lava Flows	269
6.1.4	Dark Mantle Deposits	272
6.1.5	Domes and Cones	274
6.1.6	Ridges	276
6.1.7	Sinuuous Rilles	278
6.1.8	Straight and Curved Rilles	282
6.2	Mare Basalt Rock Types	282
6.2.1	Mineralogy	284
6.2.2	Reduced Nature of Mare Basalts	292
6.2.3	Volcanic Glasses	297
6.3	Chemistry of Mare Basalts	300
6.3.1	Major Elements	300
6.3.2	Large Cations	301
6.3.3	Rare-Earth Elements and the Europium Anomaly	308
6.3.4	High Valency Cations	309
6.3.5	The Ferromagnesian Elements	311
6.3.6	Sulfur and the Chalcophile Elements	313
6.3.7	The Siderophile Elements	315
6.3.8	Oxygen and Carbon	316
6.4	Ages and Isotopic Systematics of the Mare Basalts	317
6.4.1	The Commencement of Mare Volcanism	317
6.4.2	Radiometric Ages for the Mare Basalts	318
6.4.3	Isotopic Indexes of Mantle Heterogeneity and Basalt Source Ages	320
6.5	Origin of the Mare Basalts	321
6.6	Cooling and Crystallization of the Lavas	331
6.6.1	Primary Magmas	331
6.6.2	Fractional Crystallization	333
6.7	The Record Elsewhere	335
6.7.1	Mercury—Are Basalts Present?	335

6.7.2	Mars	335
6.7.3	Venus	336
6.7.4	Io	337
6.7.5	Vesta	338
	References and Notes	338
Chapter 7 Planetary Interiors		343
7.1	The Advantages of Geophysics	343
7.2	Radii, Densities and Moments of Inertia	343
7.3	Lunar Center of Mass/Center of Figure Offset	344
7.4	Gravity	345
7.4.1	Lunar Gravity	345
7.4.2	The Mascons	350
7.4.3	Mars	352
7.4.4	Venus	354
7.5	Seismology	354
7.5.1	The Lunar Record	354
7.5.2	The Martian Record	356
7.6	Internal Structures	356
7.6.1	The Moon	356
7.6.2	A Lunar Core?	358
7.6.3	Mars, Venus and Mercury	359
7.7	Heat Flow and Internal Temperatures	361
7.7.1	Heat-Flow Data	361
7.7.2	Electrical Conductivity	361
7.7.3	The Lunar Temperature Profile	362
7.8	Magnetic Properties	364
7.8.1	Lunar Magnetism	364
7.8.2	Remanent Magnetism	364
7.8.3	Lunar Magnetic Field Paleointensities	366
7.8.4	Crustal Magnetic Anomalies	367
7.8.5	Origin of the Lunar Magnetic Field	368
7.8.6	Planetary Magnetic Fields	370
	References and Notes	372
Chapter 8 The Chemical Composition of the Planets		375
8.1	The New Solar System	375
8.2	The Type 1 Carbonaceous Chondrites (C1)	380
8.3	The Earth	381
8.3.1	Primitive Mantle (Mantle Plus Crust)	381
8.3.2	The Crust	389
8.4	The Moon	390

8.4.1	The Highland Crust	390
8.4.2	The Mare Basalts	393
8.4.3	Bulk Moon Compositions	395
8.4.4	Earth-Moon Comparisons	396
8.5	The Planets	402
8.6	Meteorite Parent Bodies and Satellites	404
	References and Notes	405
Chapter 9	The Origin and Evolution of the Moon and Planets	409
9.1	The Beginning	409
9.2	Initial Conditions in the Solar Nebula	411
9.3	Primary Accretion Models and “Condensation” in the Nebula	415
9.4	Variations Among Refractory, Volatile, Chalcophile and Siderophile Elements	417
9.5	Early Solar Conditions	418
9.6	Secondary Accretion Process	420
9.7	Formation of the Moon	423
9.8	The Formation of the Earth	429
	References and Notes	431
Chapter 10	The Significance of Lunar and Planetary Exploration	435
10.1	The Lunar Experience	435
10.2	Future Missions	436
10.3	Man’s Responsibility in the Universe	438
	References and Notes	439
Appendix I	Reference Abbreviations	443
Appendix II	Lunar Primary Data Sources	446
Appendix III	Diameter and Location of Lunar Craters Mentioned in the Text	450
Appendix IV	Lunar Multi-ring Basins	454
Appendix V	Terrestrial Impact Craters	455
Appendix VI	Appendix to Table 8.1: Sources of Data	458

Appendix VII	
Element Classification, Condensation Sequences	460
Appendix VIII	
Chondritic Rare Earth	462
Appendix IX	
The Lunar Sample Numbering System	463
Appendix X	
Planetary and Asteroidal Data	464
Appendix XI	
Satellite Data	465
Glossary	467
Index	475

Chapter 4

PLANETARY SURFACES

4.1 The Absence of Bedrock

A striking and obvious observation is that at full Moon, the lunar surface is bright from limb to limb, with only limited darkening toward the edges. Since this effect is not consistent with the intensity of light reflected from a smooth sphere, pre-Apollo observers concluded that the upper surface was porous on a centimeter scale and had the properties of dust. The thickness of the dust layer was a critical question for landing on the surface. The general view was that a layer a few meters thick of rubble and dust from the meteorite bombardment covered the surface. Alternative views called for kilometer thicknesses of fine dust, filling the maria. The unmanned missions, notably Surveyor, resolved questions about the nature and bearing strength of the surface. However, a somewhat surprising feature of the lunar surface was the completeness of the mantle or blanket of debris. Bedrock exposures are extremely rare, the occurrence in the wall of Hadley Rille (Fig. 6.6) being the only one which was observed closely during the Apollo missions. Fragments of rock excavated during meteorite impact are, of course, common, and provided both samples and evidence of competent rock layers at shallow levels in the mare basins.

Freshly exposed surface material (e.g., bright rays from craters such as Tycho) darken with time due mainly to the production of glass during micro-meteorite impacts. Since some magnetic anomalies correlate with unusually bright regions, the solar wind bombardment (which is strongly deflected by the magnetic anomalies) may also be responsible for darkening the surface [1]. Infrared and radar mapping from the Earth revealed many "anomalies" or "hot spots" on the lunar surface [2]. The regions around young ray craters show high eclipse temperatures and scatter radar signals strongly. These properties correlate with, and are caused by, the block fields surrounding

young craters. The anomalies fade into the average lunar surface values with increasing age. A corollary is that fracturing and destruction of fresh rock surfaces by impacts must be a common lunar process [2]. On Mars, the mantling effect of wind-deposited fine material likewise hampers direct observations of bedrock, except perhaps at high elevations. The summit calderas of Olympus Mons (Fig. 2.23b) may be an excellent sampling locality, possibly free of regolith or dust. The megaregolith is dealt with in Chapter 5 on planetary crusts (Section 5.1.2).

4.2 The Extreme Upper Surface

Observations are restricted mainly to the lunar surface. Measurement of conductivity indicates that the top layer is strongly insulating [3]. The exposure of lunar soils to humid terrestrial atmospheres causes large changes in the dielectric constant [4]. Curiously, the electrical properties of the surfaces of Mercury, Mars and Venus appear to be very similar to those of the Moon [3, 5]. This is readily understandable for Mercury which lacks an atmosphere and resembles the Moon in many respects. It also appears that water is not affecting the surface electrical properties of Mars, where the temperatures and pressure at the surface are usually below the triple point for water. Local exceptions may be found on Mars where the daytime temperature rises high enough for liquid water to exist on the surface, and local freeze-thaw conditions may exist. The presence of subsurface ice, permafrost and hydrated minerals may change conductivity at deeper levels [6]. On Venus, in contrast, the temperatures and pressures are far above the critical point for water [3] so that on all the inner solar system bodies (except the Earth), liquid water does not affect the electrical properties of the top surface layer.

The temperature on the lunar surface increases by about 47° K in the top 83 cm. The top surface (2–3 cm) is a loosely packed porous layer. Surface temperatures vary considerably. At the Apollo 17 site, the surface reaches a maximum of 384° K (111°C) and cools to 102° K (–171°C) at the end of the lunar night [2]. The near-surface temperature is 216° K (–57°C). At the Apollo 15 site, these temperatures are about 10° K lower. The agreement with previous estimates based on terrestrial observations was very close [8, 9].

The temperature range at the Viking sites on Mars was between 150° K (–123°C) and 240° K (–33°C) [7]; Mercury temperatures range from 93° K (–180°C) to 700° K (430°C) and surface temperatures on Venus are about 720° K (450°C).

The question of the lateral movement of the surface layer or of underlying layers has been extensively discussed (e.g., [10]). Although much material has been redistributed by impact processes (e.g., Figs. 2.1, 2.14), the underlying bedrock is the dominant influence on the composition of the regolith. The

truth of this statement is apparent from the chemistry of the soils at the various sites, with minor exceptions [11]. The chemical data from the orbital experiments (Al/Si, Mg/Si, and the gamma-ray Th values) show breaks generally coincident with the mare-highland boundaries [12]. Thus, movement of a surficial layer occurs only on a local scale, and the chemistry and nature of the regolith is dominated by local bedrock components.

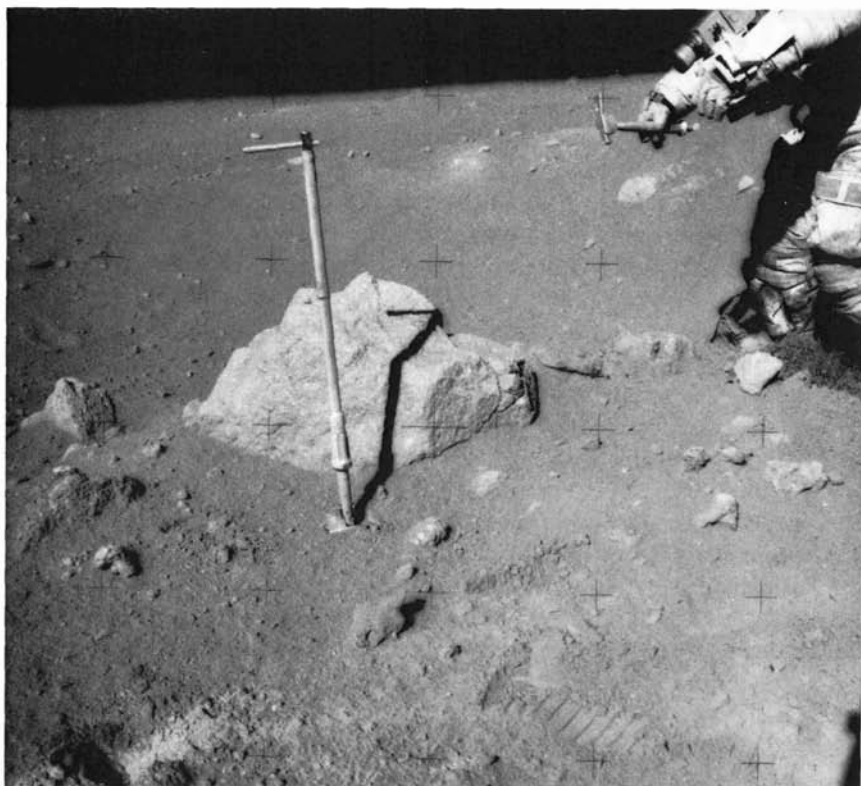
Evidence for local stirring of the very top dust layer has been deduced from the light scattering observed at the terminator by the Apollo 17 astronauts [13]. These observations are consistent with effects observed by Surveyor 6 and Lunokhod 2, and are perhaps due to dust levitation caused by temperature changes at the terminator [13, 14]. The effect does not produce any widespread migration of dust, which would blur the sharp mare-highland boundaries observed by the orbital chemical analyses [12]. Chemical and isotopic processes occurring in the upper layer of the regolith are discussed further throughout this chapter.

The importance of the very top layer in cosmic ray, solar flare, and track studies has led to the development of new sampling techniques. One such device consists of a free-floating cloth-covered plate designed to sample the top 100 micron layer. Another, a spring-loaded cloth-covered plate, sampled the top 0.5 mm [15]. Other samples in this category, from the Apollo 16 highland site at Descartes, include top and bottom samples from a boulder and soil samples from shadowed areas. Work on this material is still in progress.

Direct stereo photography with 80 micron resolution at the surface was carried out by the astronauts on the Apollo 11, 12 and 14 missions [16]. The astronauts' comments that the upper surface resembled a beach following a heavy rain shower were interpreted as the effect of micrometeorite bombardment.

4.3 The Regolith

The regolith is the continuous layer, usually several meters in thickness, which covers the entire lunar surface [17]. It is a debris blanket in every sense of the term, ranging from very fine dust to blocks several meters across (Fig. 4.1). Although the finer components (< 1 mm) are often referred to as soil, the distinction from terrestrial soils, formed by the complex interaction of the atmosphere and biosphere on rocks, is complete. The active processes on the Moon at present are cosmic, not planetary. Bombardment of the surface occurs at all scales from impacts which produce craters such as Tycho and Copernicus to erosion by particles producing sub-micron-sized pits, while cosmic ray and solar flare particles produce effects on an atomic scale. The surficial material is saturated with solar wind gases.

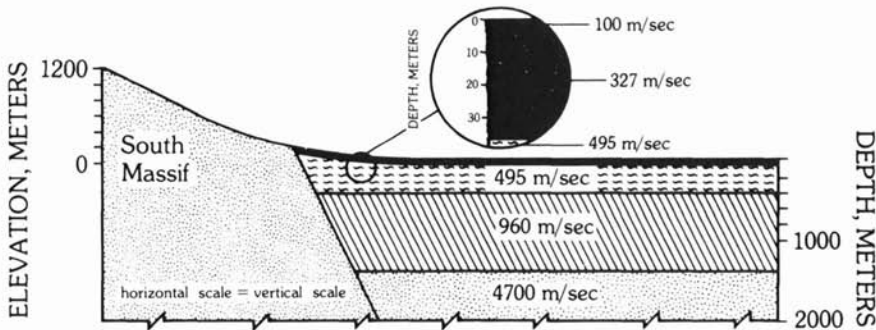


4.1 The regolith at Station 8, 3.4 km northeast of South Ray crater (Apollo 16 site). The boulder is the source of gabbroic anorthosite samples 68415 and 68416 (NASA AS-16-108 17697).

4.3.1 Thickness and Mechanical Properties

The thickness of the regolith has been established mainly by observations of those craters that are seen to excavate bedrock, and by direct observations along the edge of Hadley Rille [18]. Here, the base is seen to be irregular. The average thickness of the regolith on the maria is 4–5 m, while the highland regolith is about twice as thick (averaging about 10 m), due both to a longer exposure history and to a more intense meteorite flux.

The regolith, although quite variable locally in thickness, has very similar seismic characteristics at all sites (highlands and maria alike), typically with very low seismic velocities of about 100 m/sec [19] (Fig. 4.2). The value ranges over the different Apollo sites (Apollo 12–17) from 92–114 m/sec, indicating that the processes producing the regolith formed material of uni-



4.2 A cross-section of the regional structure at the Apollo 11 landing site in the Taurus-Littrow valley [19].

form seismic properties moon-wide from different mare and highland source materials. The seismic velocities increase rapidly below the regolith. At the Apollo 17 site the velocity reaches 4.7 km/sec. at a depth of 1.4 km. That is good evidence that the subsurface material is not dust but basaltic flows, fractured near the surface and underlying a few meters of regolith. This conclusion is strengthened by the orbital radar evidence for basin-wide subsurface reflectors at depths of 0.9 and 1.6 km in Mare Serenitatis, and at 1.4 km in Mare Crisium [20].

There are many local variations in regolith thickness. Perhaps the most extreme example is in the Taurus-Littrow Valley where, near the landing site, thickness ranged from 6.2 to 36.9 m. It can be argued that such changes are due to the local concentration of medium-sized craters (such as Camelot, 700 m in diameter) producing uneven thicknesses due to local throwout, burying smaller craters.

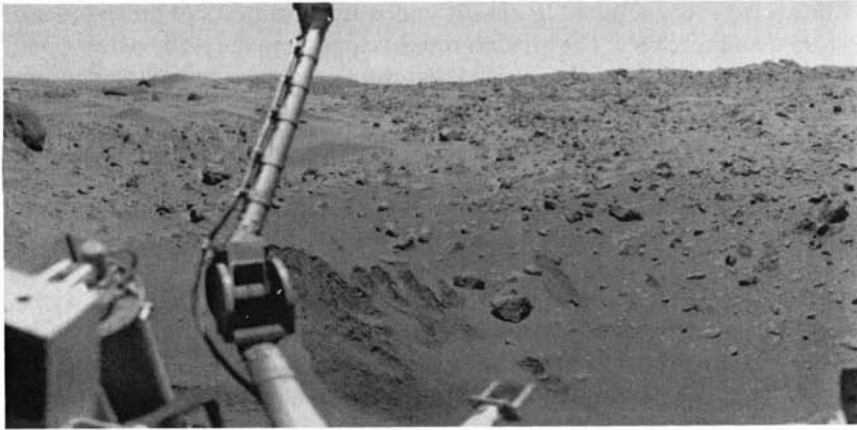
Regolith thicknesses on the Cayley Plains at the Apollo 16 site vary between 6 and 10 m, but may be up to 20 m on the Descartes Mountains [21]. Regolith development on the rims of young craters is very limited. The thickness on the rim of North Ray crater (Apollo 16 site) is only a few centimeters. North Ray crater is 50 million years old [22] (Fig. 4.3).

The bulk density of the soils ranges from 0.9 to 1.1 g/cm³ at the top surface, but increases with depth to values up to 1.9 g/cm³. The density increases markedly in the upper 10–20 cm [23, 24]. The porosity of the upper surface is 45%, with higher values around crater rims, as judged from soil mechanics studies of the astronauts' footprints. Thus, the top surface is very loose, due to stirring by micrometeorites, but the lower depths, below about 20 cm, are strongly compacted, presumably by shaking during impacts. The compressibility of the soil is similar to that of ground-up terrestrial basalt.



4.3 North Ray crater, 900 m in diameter, viewed from Station 11 at the Apollo 16 Descartes site. The regolith on the rim of this 50-m.y.-old crater is only a few centimeters thick (NASA AS-16-116 18599).

All of these mechanical properties, vital for manned landings and astronaut surface activities, have been extensively studied [23, 24]. Notwithstanding the differences in composition, particle size and shape, and grain size distribution, from a soil mechanics or engineering point of view the lunar soil does not differ significantly in its behavior from what would be expected on Earth of granular, slightly cohesive terrestrial soil with the same particle size distribution and packing characteristics. The one major difference that might be singled out is the interparticle adhesion of lunar soil, which is demonstrated, for example, by the sharp vertical walls produced by the indentation of the footprints and by the difficulty of handling lunar powders in the laboratory.



4.4 View of the Martian surface from the Viking 1 lander in Chryse Planitia.

The similarity of lunar soil in mechanical properties to those of terrestrial examples is due to the fact that the mechanical properties depend on size, density, and shape of the particles rather than on their chemical composition. The consensus from the soil mechanics studies [24] and from the seismic data [19] is that the mechanical properties of the lunar soils are about the same at all sites. With the exception of two photographs of the Venusian surface, Mars is the only other body in the solar system for which we have some detailed knowledge of the nature and properties of its surface (Fig. 4.4). The clarity of the photographs enables unambiguous interpretations to be made. The surface layer appears to be firmer than that of the lunar regolith [7]. The fine-grained material is strongly adhesive, like the lunar fines. Bulk density is about 1.2 gm/cm^3 . Small weakly cohesive clods are common and the soil contains many more large rocks than the lunar regolith. The presence of dunes indicates substantial wind transport and fine material will thus be selectively removed. Remote sampling of such material would not yield the fragments of rocks commonly found in the lunar soils.

4.3.2 Structure

The layered nature of the regolith has now been revealed by many core samples. A total of 26 core samples of varying depths up to 3 m were taken during the missions, along with many scoop samples of soil. The cores provided valuable data after some initial confusion due to the early sampling techniques, which did not return undisturbed cores. The deepest core (294.5 cm) was at Apollo 17. Core tube samples from Apollo 11, 12, and 14 missions produced disturbed samples, but on Apollo 15, 16, and 17 missions, use of

thin-walled tubes resulted in almost undisturbed samples of lunar soil with 90–95% core recovery. The greatest insight came from the study of the Apollo 15 deep core, which clearly revealed that the regolith was not a homogeneous pile of rubble. Rather, it is a layered succession of ejecta blankets. An apparent paradox is that the regolith is both well mixed on a small scale and also displays a layered structure. For example, the Apollo 15 deep core tube, 242 cm long, contained 42 major textural units ranging from a few millimeters to 13 cm in thickness. There is no correlation between layers in adjacent core tubes and the individual layers are well mixed.

This paradox is resolved as follows. The regolith is continuously gardened by meteorites and micrometeorites. Each impact inverts the microstratigraphy and produces layers of ejecta, some new and some containing remnants of older layers. The new surface layers are stirred by micrometeorites.

A complex layered regolith is thus built up, but is in a continual state of flux. Particles now at the surface may be buried deeply by future impacts. In this manner, regolith is turned over like a heavily bombarded battlefield. The layering in a core tube has no wider stratigraphic significance. It is local and temporary. The result is that we have the well-stirred and homogeneous regolith, with one portion very like another, uniform moon-wide, as shown by the seismic data, yet layered locally.

These processes have been placed on a quantitative basis [25, 26]. The most important result is that the turnover rate of the regolith decreases rapidly with depth. "While it takes approximately 10^7 yr. to excavate the regolith at least once (with 99% probability) to a depth of 9 mm, it will take 10^9 yr. to excavate to a depth of 7 cm; simultaneously, however, the uppermost millimeters of the regolith has [sic] been turned over approximately 700 times in 10^7 yr. and many thousands of times in 10^9 yr." [26, p. 9].

The upper one millimeter of the regolith is the zone where most reworking and mixing by micrometeorites occurs on these models. There is some indication from measurements of cosmogenic radionuclides that these depth estimates may be too low. Thus, studies employing ^{53}Mn (half-life of 3.7 million years) on the Apollo core samples [27] indicate a mean depth of disturbance, over 10^7 yr. to be about 5–6 g/cm² (about 3 cm). The difference between these two estimates depends partly on the mass distribution of the impacting bodies, but also indicates the difficulties in modelling these processes.

The calculations with respect to vertical mixing within the regolith, discussed above, are much more readily treated than are the problems of local and exotic components in the regolith at a particular landing site. Lateral transport is not particularly efficient; otherwise, the regolith would be laterally homogeneous over broad areas. This lack of homogeneity is reflected in the fact that the admixture of mare and highland soils close to geological boundaries is surprisingly small. Mare-highland contacts appear relatively

sharp on orbital geochemical data. At the Apollo 15 and 17 sites, steep chemical and petrological gradients in soil compositions occur over distances of a few kilometers. According to early calculations, about five percent of the regolith at a site may be derived from distances greater than 100 km, while 0.5 percent come from distances greater than 1000 km. Fifty percent comes from distances less than 3 km [28–30]. Thus, most of the regolith is of local origin. In accordance with the predictions, components of the Apollo 11 soil sample were derived from highland sources, leading to the identification of the highlands as “anorthositic” [31]. However, Hörz [26, p.11] has drawn attention to the apparent anomaly that most genuine mare soils (e.g., Apollo 11, 12 and Luna 16) contain 10–30% of non-mare material, and that this is constant over wide areas of mare soils, increasing only within 5 km of exposed highlands. A current problem is whether such material is derived from highland material at shallow depths beneath the mare basalts.

4.3.3 Rate of Accumulation

The accumulation rate for the past three aeons of the lunar regolith averages about 1.5 m per aeon [32], 1.5 mm per million years, or about 15 angstrom units per year corresponding to a layer of about 6 oxygen anions. However, such averages are misleading. The accumulation of the regolith occurs as a result of the addition of discrete layers, and is not continuous. The local accretion rate is extremely variable. In comparison with terrestrial erosion and deposition, lunar processes are slow indeed.

The accumulation rate, which is directly related to the meteoritic cratering flux (Section 3.16), steepens appreciably in the period between 3.5 and 4 aeons. The present regolith in the highlands dates from about 3.8 to 4.0 aeons, which marked the close of the intense bombardment, culminating in the impacts that formed the Imbrium and Orientale ringed basins. The accumulation rate for the period 3.5–4.0 aeons is about an order of magnitude greater than in younger epochs. A complicating factor is that the regolith does not grow at a constant rate, even if the meteorite flux is steady [25]. As the regolith increases in thickness, it buffers the bedrock against the smaller impacts. Larger impact events are thus required to generate fresh bedrock debris. With increasing regolith thickness, samples from deeper source areas will be added to the top surface [25].

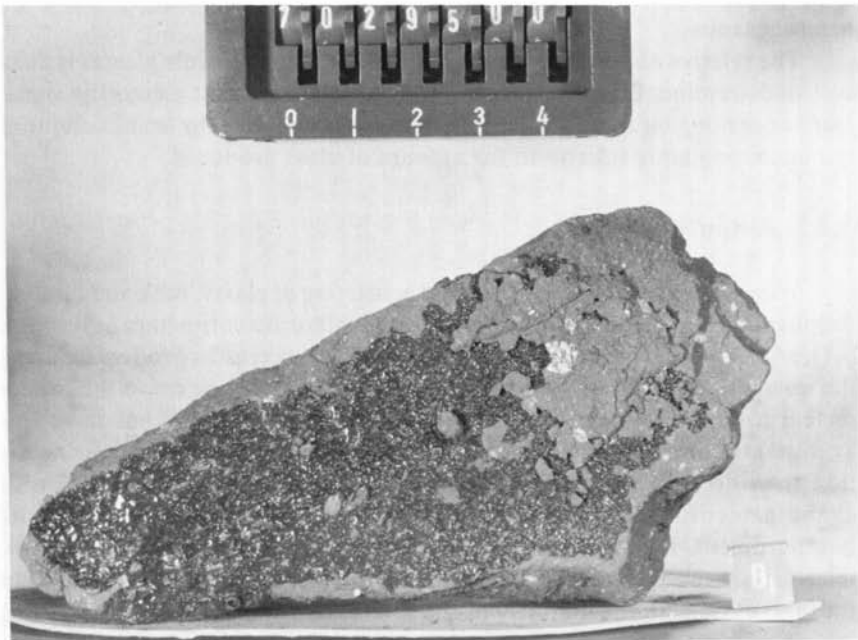
4.3.4 “Ages” of the Soils

The exceedingly complex mixture represented by the soil contains components of varying ages. This was dramatically emphasized by the apparent paradox from initial investigations that the mare soils had model Rb-Sr ages around 4.6 aeons, although they were lying on and principally derived from

pages 124 – 126 deleted

4.3.5 Soil Breccias and Shock Metamorphism of Lunar Soils

Soil breccias, consisting of weakly indurated mixtures of rock fragments (Fig. 4.7), glass and fine soil, achieved an undue early prominence by comprising about half of the initial Apollo 11 sample return. Experimental work has shown that single meteorite impacts into soil can produce these breccias [38]. Using a 20 mm powder gun to simulate shock pressures between 150 and 730 kbars, the lunar soil was compacted and partially remelted to form agglutinates and soil breccias. *In situ* melts of agglutinates and melts along grain edges occur at low pressures. The highest pressure shock melts are closest in composition to the bulk soil composition. Propagation of shock waves from a single impact in soils causes collapse and shear of grains, collapse of pore spaces, and compaction which indurates the soil at low pressures (150–180 kbars) with less than 5% melting. These resemble soil breccias. As the pressure increases, the amount of intergranular melt and shock melting increases. Above 650 kbars, 30–75% of the sample melts, producing a pumiceous glass. Thus, the formation of soil breccias does not require sintering in hot base surge deposits [39] or repetitive impacts [40].



4.7 Soil breccia 70295 showing glass coating (NASA S-73-17192).

4.4 Glasses

Many varieties of glasses are found in the lunar soils. The existence of the glasses is mostly due to melting during meteorite impact, but some important exceptions occur. The emerald green glass from Apollo 15 provides us with a primitive basaltic composition. The orange glasses from Taurus-Littrow (Apollo 17) contribute to our knowledge of the dark mantle and of the mechanism of mare basalt eruption. These and other glasses of possible volcanic origin are discussed in Chapter 6 on basaltic volcanism (Section 6.2.3). The emphasis here is on the common and abundant impact-derived glasses.

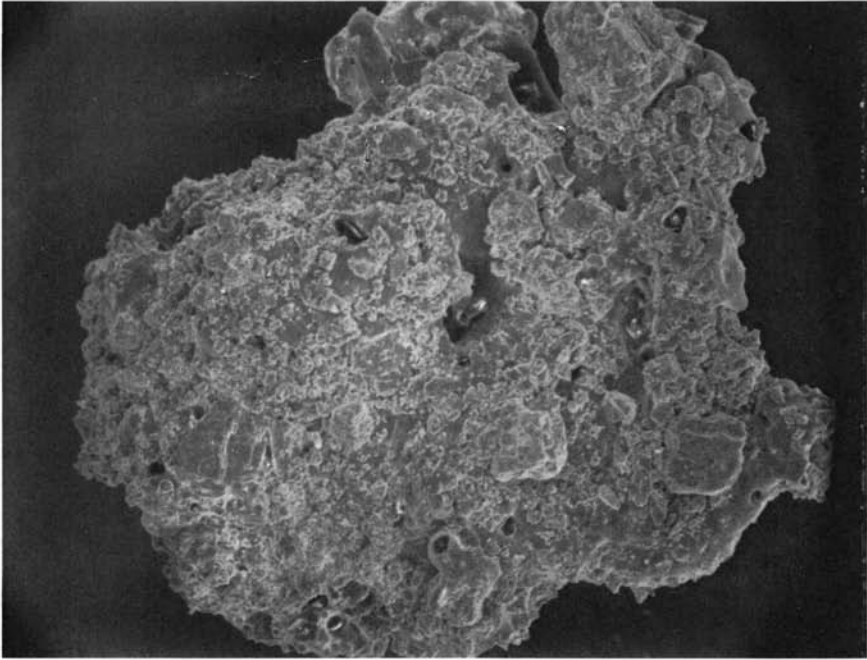
Because the more spherical varieties of the glasses are abundant and generally homogeneous, they are suited to chemical analysis by electron microprobe techniques. This enables estimates to be made of the frequency of various chemical compositions, which may then be related to the parental rocks. This approach is important for the heavily cratered and brecciated highlands, where terrestrial petrographic experience and techniques have been less readily adapted to lunar studies than was the case with the mare basalts. However, in these studies, care must be taken to avoid bias and the identification of mixtures as primary rock types. There are many non-homogeneous glasses, while the agglutinates (Section 4.4.1) are particularly heterogeneous.

The relative abundance of impact-produced and volcanic glasses is difficult to determine. Even the absence of siderophile element meteoritic signatures does not guarantee a volcanic origin, on account of the small volume of the impacting body relative to the amount of glass produced.

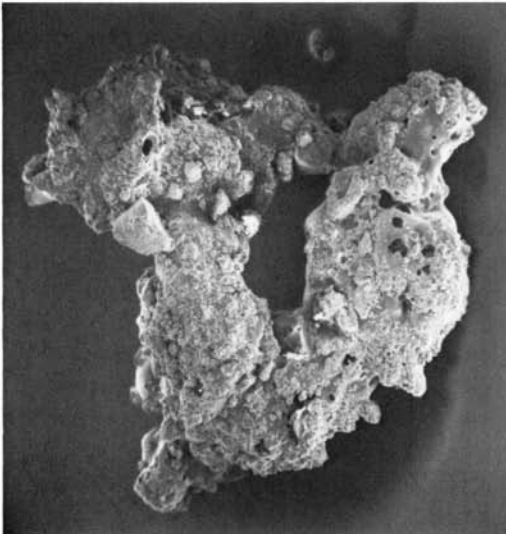
4.4.1 Agglutinates

These are glass-bonded aggregates consisting of glassy, rock and mineral fragments (Figs. 4.8, 4.9). They form during micrometeorite impact into soil [41], and may be in part the remnants of small glassy craters produced during the impacts. Their abundance in a soil is an index of exposure to the micrometeorite bombardment and hence of soil maturity. Soils that have low agglutinate contents contain evidence of a shorter exposure to cosmic radiation than do soils with a high agglutinate content [42]. The formation of agglutinates offsets the grinding up of the soil particles by the micrometeorite bombardment. Eventually an equilibrium grain size in the soils of about 60 microns is reached by these two competing processes. The agglutinate content thus increases with the maturity of the soil.

In general, the average composition of the glassy portion of agglutinates is that of the soil in which they were formed, providing the soil is mature. Accordingly, such compositions may be used in complex regoliths to deter-



4.8 SEM photo of an Apollo 12 agglutinate, consisting of lithic, mineral and glassy debris bonded together by inhomogeneous glass. Width of photo is 1 mm. (NASA S.70 34983. Courtesy D. S. McKay.)



4.9 SEM photo of a 1-mm Apollo 12 agglutinate particle. (NASA S71-24575. Courtesy D. S. McKay.)

mine fossil soil compositions. For example, at the Apollo 17 site, it is possible to calculate the contribution to the regolith from the landslide at the South Massif. Pre-Camelot crater soils and pre-central cluster soils can also be identified by this approach [43]. These considerations place some restrictions on mixing calculations for soils. It is clear that such chemical calculations should always be accompanied by petrographic examination of the soils, particularly in areas such as the Apollo 17 regolith where agglutinates formed from mature soil compositions may be mixed with freshly excavated material [43].

For some time, it was thought that major elemental fractionations occurred during the formation of agglutinates [44]. Detailed analysis of agglutinate fractions separated by magnetic separation techniques showed increases in the concentration of the ferromagnesian elements (Fe, Mg, Ti) and decreases in the abundances of Na, Ca, Al and Eu, typical constituents of plagioclase. These effects were attributed to selective melting of pyroxene during agglutinate formation, relative to the more refractory plagioclase. However, like other impact-produced partial melting scenarios on the Moon, this effect is not real. The magnetic separation processes used to separate the agglutinate fractions were biased not only toward magnetic agglutinates, but also select magnetic non-agglutinates (e.g., pyroxenes, ilmenites and olivines with included Fe-Ni grains). The non-magnetic residue was selectively enriched in non-magnetic agglutinates, including plagioclase compositions. Accordingly, the proposed chemical fractionations were an artifact [45]. It has been proposed that agglutinates form by preferential fusion of the finest (<10 micron) fraction of the soils [46] but this model requires much testing before it can be substantiated.

4.4.2 Impact Glasses

Many different forms have been described. The spheres are typically about 100 microns in diameter, but range widely in size. Ellipsoidal shapes, dumbbells, teardrops, and rods, are common (Figs. 4.10, 4.11). These are the typical rotational shapes assumed by splashed liquids. Some of the spheroidal forms are flattened, indicating that they were plastic when they landed. There is a great abundance of angular fragments. Many of these are broken pieces of the more regular forms. Others occur as large irregular masses (>10 g) coating rocks or as linings in pits clearly produced by impact of small particles. The outer surfaces of the spherules commonly have small craters.

A wide range in color is shown by the glasses from colorless through pale yellow, green, brown, orange to red, and black. The colors show a clear relation to refractive index and to composition. Table 4.1 shows the interrelationship of color, refractive index and density. (See also Section 6.2.3 on the emerald green and orange glasses.) The color of the glasses is clearly reflected

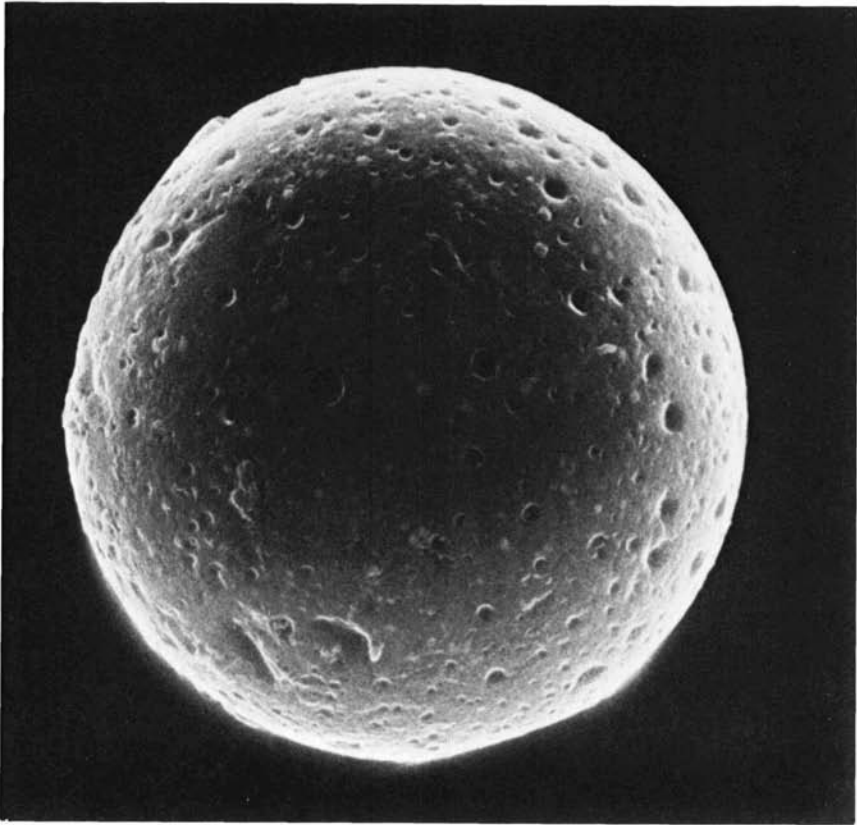


4.10 Ropy glass fragment, 1 mm long, of KREEP glass (12033). (NASA S.70 17107. Courtesy D. S. McKay.)

in the chemistry. The lighter colored glasses are similar in composition to the feldspathic or anorthositic fragments, whereas the more numerous red, yellow and dark brown glasses resemble the bulk analyses of the rocks and the fine material.

Tiny spherules of iron are present in many of the glasses. They are normally less than 30 microns in diameter and are especially frequent in the heterogeneous glasses. Some of these spherules contain about 10% Ni as well as troilite and schreibersite, which are common minerals of iron meteorites.

Others, probably the majority, are derived by auto-reduction of Fe^{2+} (see Section 4.5.1). These contain nickel-free iron and troilite derived from the lunar rocks, forming immiscible droplets in the glass melt. The chief evidence for an external meteoritic origin for the nickel-rich iron spheres is their nickel content, since nickel is very depleted in the parental rocks. These nickel-iron spheres resemble those found in terrestrial glasses that have been formed at meteorite craters by the fusion of country rock by the impacting iron-nickel meteorite. The presence of these globules indicates that most of the glasses



4.11 SEM photo of Luna 24 glass sphere, showing some superficial resemblance to Tethys. The pits are due to removal of included iron spherules, and not to impact. (NASA S.78-36991. Courtesy D. S. McKay.)

Table 4.1 Relationships between color and other properties of lunar glasses.[†]

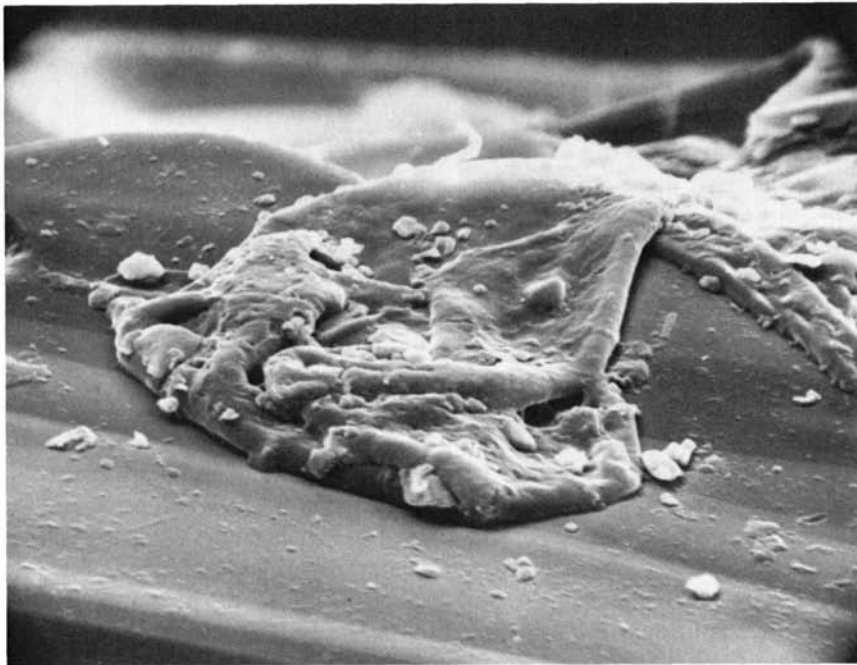
Color	Refractive Index	TiO ₂ (%)	FeO (%)	Density
Colorless, transparent	1.50–1.60	0–0.1	0–1.6	< 2.7
Light yellow, green to light green, transparent	1.59–1.65	0.1–2	4–10	2.7–2.8
Dark green, transparent	1.65	0–1	7–16	2.8–2.9
Yellow-brown, transparent	1.65	1–2.5	8–14	2.7–2.8
Light to dark brown and red-brown, transparent	1.65–1.75	3–8	9–16	2.8–3.0
Dark brown to opaque	1.75	7–12	15–25	3.0–3.25

[†]From Frondel, C. (1970) *PLC 1*: 450.

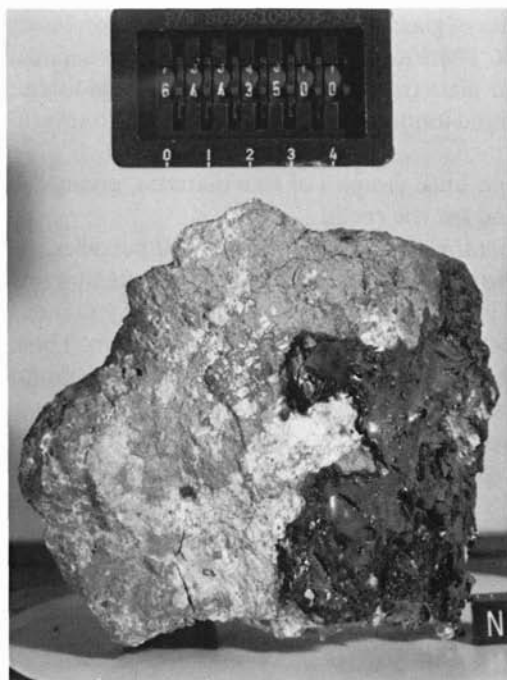
bear a genetic relationship to meteorite impact. Most of the surface features, such as small craters, pits, splashes of glass (Figs. 4.12a and b) and iron beads are the result of meteorite impact. There are no major differences in chemical composition between the angular glass fragments and the spheroidal forms.

The range in composition found among the glasses can be due to several causes:

- (a) Melting of whole rocks and bulk samples of fine material, giving the range in composition found for the rocks.
- (b) Melting of individual mineral phases by impact of small particles.
- (c) Selective vaporization. The overall evidence seems to indicate that this process was not effective in altering the composition to any marked degree. Studies from terrestrial glasses support this contention. Thus, at the Lonar Crater, India, the glasses are identical in composition to the parental basalts [47] supporting similar conclusions for impacts into terrestrial sedimentary rocks [48]. Evidence of rather thorough mixing to produce homogeneous glasses from diverse target rocks occurs at large terrestrial impact sites, such as Manicouagan [49]. This question becomes important in studying the highland samples, where most of the evidence for primary rocks has to be inferred.



4.12a Glass splash on a lunar olivine crystal. The width of the "lava flow" is 100 microns. (NASA S.71 24637. Courtesy D. S. McKay.)



4.12b Glass coating Apollo 16 lunar breccia 64435 (NASA S.72-39674).

- (d) Selective melting of specific minerals; e.g., under shock conditions, feldspar melts at lower pressures than does pyroxene or olivine.

Although there are some similarities in form between the spherules and chondrules observed in chondritic meteorites, detailed textural studies of chondrules [50, 51] do not provide many direct analogies, and do not directly support an origin for chondrules in a lunar-type regolith. The chondritic meteorites are, of course, different in composition from the lunar breccias, and there is ample evidence from the Apollo studies that the chondritic meteorites are not derived from the Moon.

A final observation concerning the resemblance between some glass forms and microfossils deserves wide circulation: "The abundant spheroids and ovoids are similar in shape to some algal and bacterial unicells, and the smaller ones are comparable in size. Indeed, if such particles were coated with carbon, they would make impressive pseudomicrofossils . . . This is not to propose that there are or were solid glass Protozoa on the Moon, but to add one more warning about a too-ready interpretation of exotic objects as of vital origin on the basis of gross morphology alone . . . This warning deserves emphasis. Elsewhere on the lunar or Martian surface may be lifelike artifacts that will be harder to discriminate from the real thing" [52].

pages 135 – 150 deleted

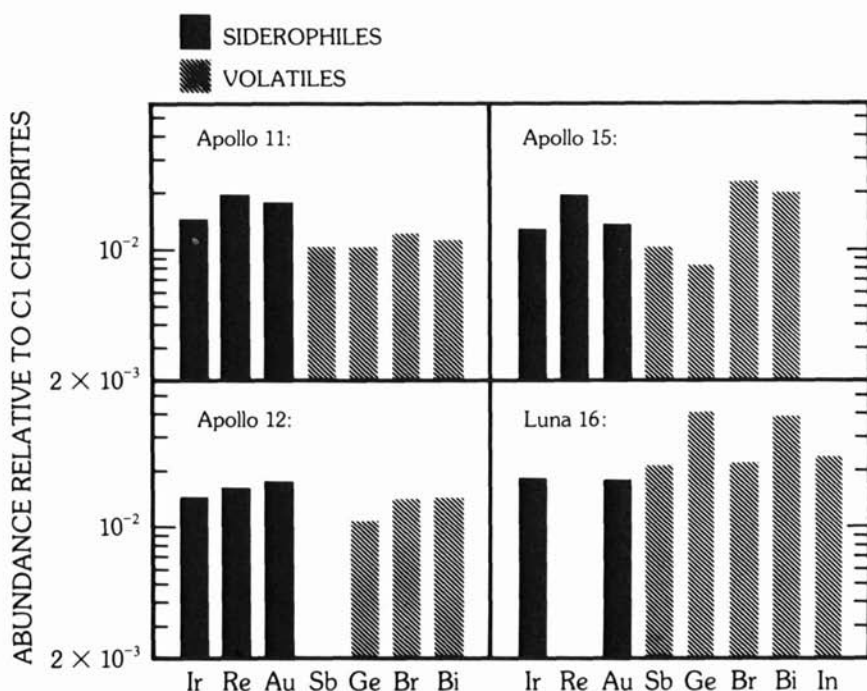
be trapped as ice in craters in polar regions [88]. The source of the water could be from solar wind hydrogen as a source for reduction of FeO, carbonaceous chondrites or cometary impacts, since no unequivocal identification of indigenous water has been made. Other suggestions include the possibility of trapped frozen gases, for example, radon-222 derived from radioactive decay of uranium [89].

4.5.3 The Meteoritic Component

Addition of meteoritic material to the Moon is derived from three sources: the ancient heavy bombardment, young crater forming events, and micrometeorites in addition to possible cometary material. In this section, the nature and composition of the meteorite contribution in the lunar regolith is explored, while the question of the nature of the basin-forming projectiles is discussed in Section 5.6. The investigation of this component was aided by two geochemical factors [90]. The first was the strong depletion of siderophile elements (e.g., Ni, Ir, Au, Re) in the lunar rocks. Such depletions are to be expected on the surfaces of differentiated planets; however, the extreme depletion of the Moon in volatile (and chalcophile) elements (Ag, Bi, Br, Cd, Ge, Pb, Sb, Se, Te, Tl, Zn) enabled the use of these elements, which are relatively abundant in CI meteorites, as indexes of the meteoritic component. Typical data are shown in Fig. 4.17 for mature soils, with high surface exposure ages. Such soils from all sites give the same result. The meteorite component appears to be similar to CI chondrites, and the concentration level is 1.5–2% by weight. There is some variability among the volatile constituents, probably due to their mobility in the soils, hence producing a sampling problem. It is of interest that this chemical signature virtually eliminates all the other meteorite classes (irons, stony irons, ordinary chondrites, achondrites) from consideration [90, 91]. Mean influx rates have been calculated as 2.4×10^{-9} g/cm²/yr. [90] and 2.9×10^{-9} g/cm²/yr. [91]. Discrepancies between these estimates and those calculated from the microcrater population (0.2×10^{-9} g/cm²/yr.) [92], which are an order of magnitude less, are discussed in the next section.

4.6 Microcraters and Micrometeorites

The lunar surface is a particularly fine recorder of micrometeorite impacts. This arises from the ubiquitous presence in the regolith of glasses, whose smooth surfaces provide an ideal recording surface for micrometeorite impacts. Typically, these will contain about 5000 microcraters (with diameters of a few microns) per square centimeter. The number of craters decreases with increasing diameter. These microcraters or “zap pits” which occur on rock and

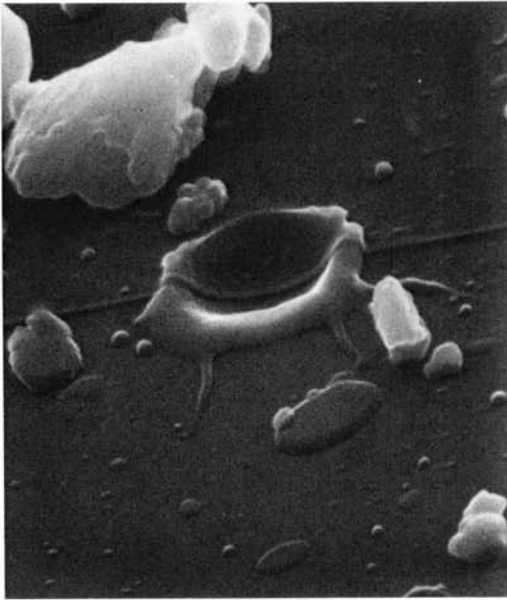


4.17 All mare soils are enriched in “meteoritic” elements, relative to crystalline rocks. Net meteoritic component is obtained by subtracting an indigenous lunar contribution estimated from crystalline rocks. Abundance pattern is flat, with siderophiles and volatiles almost equally abundant. The meteoritic component has a primitive C1 composition [90]. (Courtesy E. Anders.)

mineral surfaces, as well as on the glass spheres, are spectacular (Fig. 3.1). They range in size from less than one micron to more than one centimeter.

Information on the nature of the projectiles provides data on micrometeorite flux and on the nature and composition of “interplanetary” or “cosmic” dust. The microcraters larger than about 3 microns typically consist of a glass-lined pit, and a “spall” zone concentric to the pit (Fig. 4.18). Spallation in this zone will sometimes leave the glass-lined pit standing on a pedestal of “halo” material. The hypervelocity nature of the impacts indicates that “primary” cosmic dust particles [93] are involved rather than “secondary” particles resulting from lunar impacts [94]. Most of these microcraters are compatible only with impact velocities of the dust grains greater than 3.5 km/sec, the actual average velocity being about 20 km/sec.

What conclusions can be drawn about the nature of the particles from the crater morphology? The densities lie within the range $1\text{--}7\text{g/cm}^3$, peaking in

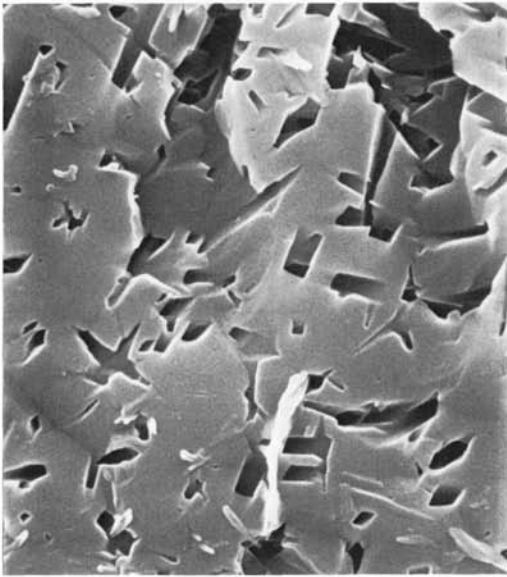


4.18 One-micron sized zap pit on a lunar glass spherule. (NASA S.73-18445. Courtesy D. S. McKay.)

the range $1\text{--}2\text{ g/cm}^3$. Thus, there is a lack of iron particles, and the composition is similar to that of Type I carbonaceous chondrites. These data are consistent with the properties of “Brownlee” particles collected by high-flying aircraft [95].

Therefore, the “model” micrometeorite is non-porous, equant in shape, with a density of $1\text{--}2\text{ g/cm}^3$ with C1 element abundances, including finely dispersed carbon. This observation has implications for theories of cosmic dust origin and early planetary condensation and accretion. The abundance of “frothy” rims on impact pits is consistent with impacts of hydrated phyllosilicates, common constituents of carbonaceous chondrites. The higher density objects (5 g/cm^3) are probably magnetite grains. The most frequent mass range for the particles is from 10^{-7} to 10^{-4} g.

Craters from 1 mm to 100 microns in diameter correspond to a mass ranging from 10^{-3} to 10^{-6} g. Those craters with diameters from 100 to 0.1 microns are caused by particles in the mass range 10^{-6} to 10^{-15} g. Those in the size range 10^{-6} to 10^{-2} g contribute the most energy and are responsible for most of the damage to the rock surfaces. The production rate is about five craters per square centimeter per million years (with diameters > 0.05 cm). Thus, surfaces are effectively saturated at about one million years, and this limits the microcrater technique for exposure-age estimation. The impacts cause erosion, ionization, vaporization, and lateral small-scale transport but little vertical mixing. The erosion rate is of the order of 1 mm per million years [96].



4.19 Etched pits, about one micron across, caused by solar flare iron group nuclei, in an Apollo 14 feldspar. The rectangular outlines of the etched pits are presumably due to crystallographic factors. (NASA S.72-55177. Courtesy D. S. McKay.)

The microcratering effects extend down from those caused by micrometeorites to sputtering by solar wind ions (Fig. 4.19). Table 4.5 indicates the density of microcraters spanning this range. The erosion rate due to the sputtering is about 10^{-8} cm (1\AA) per year in the near surface (<0.1 cm) regions, or about 0.1 mm per million years. This is about one-tenth of the mass erosion rate caused by micrometeorites.

Table 4.5 Microdensities due to micrometeorite impact and solar wind sputtering.

	Crater Diameter	Crater Density (per cm^2)
Micrometeorites	$\cong 0.3$ mm	20
	$\cong 0.1$ mm	70
Solar wind sputtering	$\cong 1$ micron	1000–3000
	$\cong 0.25$ micron	10,000

The impact velocities of meteoritic dust particles vary from 2.4 km/sec to 74 km/sec. Meteorites larger than 50 g should produce a detectable signal on the lunar seismometers [97]; however, the seismometers have not detected increased flux rates on the Moon at times when meteorite showers have been observed striking the Earth. Since most showers of micrometeorites consist of particles ranging from 1 to 10^{-6} g (F. Hörz, pers. comm, 1981), the failure to detect increased flux rates on the Moon is most likely due to the fact that only

the larger events are recorded (about one signal per day due to meteorite impact [97]).

4.7 Irradiation History of the Lunar Surface

The lunar surface is not excelled as a detector and recorder of solar and cosmic radiation over geological time scales. It is much superior to meteorites, since it has been in its present orbit for a long time, whereas the orbits and dynamical evolution of meteorites are uncertain, extending probably inside the orbit of Venus and out to the asteroid belt. The orbits of two chondritic meteorites, Pribram and Lost City, photographically recorded during entry, indicate an elliptical orbit extending to the asteroid belt. These data help to dispose of the myth that meteorites come from beyond the solar system.

Three types of radiation interact with the lunar surface. In order of increasing energy, these are: (a) solar wind, (b) solar flares, and (c) galactic cosmic rays. The composition of this radiation is similar, being mainly composed of protons, with about 10% helium nuclei and about 1% of nuclei heavier than helium. There are, however, dramatic differences in energy, by many orders of magnitude, and, accordingly, in the effects on the lunar surface. In contrast, the number of particles is inversely proportional to their energy (Table 4.6).

4.7.1 Solar Wind

The solar wind has an average velocity of 400 km/sec with an energy of about 1 keV/nucleon (Table 4.6). The average density at one Å is about 10 ions/cm³. This plasma, which continually flows outward from the sun, probably represents the composition of the solar corona. Ions are directly implanted into the surfaces of lunar materials, to depths of about 500 Å. The solar wind also causes some surface damage, resulting in some fine-scale rounding and production of an amorphous coating about 400 Å thick on the surfaces of grains [98]. The abundances of the rare gases in the solar wind, relative to hydrogen, approximate the average solar photosphere and coronal abundances [99, 100]. The composition of the solar wind, and its significance for the history of the sun, is discussed in Section 4.11.

4.7.2 Solar Flares

These have higher energies than those of the solar wind, typically in the range of 10 keV to 100 MeV/nucleon (Table 4.6). They occur as short bursts of radiation and there is some correlation with the eleven-year sunspot cycles.

Table 4.6 Nuclear particle effects in lunar samples and meteorites.[†]

Radiation Source	Proton Flux (P/cm ² /sec)	Energy	Typical Penetration Distance	Major Observable Effects
Solar wind	3×10^8	1 keV/nuc	300 Å	Direct implantation (e.g., surface correlated rare gases) Re-implantation of lunar atmospheric species (e.g., ⁴⁰ Ar excess in lunar soils) Radiation damage (e.g., amorphous layers on lunar dust grains)
Solar flares	10^2	< 1 MeV/nuc to ≥100 MeV/nuc many more low energy than high energy particles	millimeter to centimeter	Radionuclide production (e.g., ²⁶ Al, ³⁵ Mn) Track production (principally tracks produced by slowing down VH nuclei) Electronic defects (e.g., thermoluminescence)
Galactic cosmic rays	1	≥100 MeV/nuc typically ~3 GeV/nuc	centimeter to meter	Radionuclide production Stable isotope production (e.g., ²¹ Ne, ¹⁵ N) Nuclear effects due to buildup of nuclear cascades with depth (e.g., N-capture in Gd) Tracks (spallation recoils in addition to slowing down heavy nuclei)

[†]Adapted from Walker, R. M. (1980) *Ancient Sun*, p. 11.

Solar flares produce three identifiable effects: (1) directly implanted ions, (2) cosmogenic nuclides and (3) nuclear tracks.

The Apollo missions were well timed. Large solar flares occurred in November, 1968, and April, 1969, before the Apollo 11 mission in July, 1969. Large flares were absent before the Apollo 15 mission. A small solar flare, which enhanced the particle flux by a factor of 10^3 , occurred during the Apollo 16 mission. In August, 1972, before the December, 1972, Apollo 17 mission, the most intense solar flares observed during the past fifteen years occurred. Tracks produced by solar flares dominate the upper one millimeter of lunar materials that have been exposed directly to sunlight. These track densities are high (10^7 – 10^9 /cm²).

4.7.3 Galactic Cosmic Rays

These very high energy particles (10^2 – 10^4 MeV/nucleon) are derived from outside the solar system (Table 4.6). These particles are not implanted in the lunar surface materials since they undergo nuclear interactions due to their high energies. Cosmic ray tracks are produced by the VH ions ($Z = 18$ – 28) and VVH ions ($Z > 28$), while the lighter nuclei (protons and He nuclei) produce both stable and radioactive isotopes.

There are two main classes of phenomena which result from the interaction of cosmic rays with the lunar surface: (a) solid-state damage as a result of penetration of ionizing particles, producing etchable tracks, and (b) production, through nuclear interactions, of new isotopic species. These effects have been pursued by different investigators using etching and microscopic techniques to study the tracks produced, and mass spectrometric and radiochemical procedures to investigate the cosmogenic isotopes.

4.8 Physical Effects of Radiation

The solar wind causes only minor damage, as noted earlier, producing amorphous surface layers a few hundred angstrom units thick on grain surfaces. Helium nuclei are thought to be mainly responsible [101–103]. The time needed to produce this amorphous layer is about 100 years. Solar flares, in contrast, produce high track densities, sometimes exceeding 10^{11} tracks/cm². These are observed even in the deepest core samples, indicating that this material was once at the surface. Such tracks are also observed in gas-rich meteorites [104], although both track densities and the number of grains irradiated by solar flares are less, consistent with much lower rates of surface overturn (gardening) on asteroidal surfaces compared with the lunar regolith.

The tracks produced by galactic cosmic rays are mostly caused by the heavier ions, dominated by the VH ions ($Z = 18$ – 28) of which iron is the most

abundant species [105]. The track densities fall off steeply with depth, but tracks due to cosmic rays may reach depths of 20 cm or so, in contrast to the predominance of tracks from low energy solar flare ions in the upper one millimeter. Track lengths differ in differing minerals, in the order feldspar > pyroxene > olivine. The tracks are produced only toward the end of the penetration.

Workers have used either the total etchable track length or the track etch rate to identify the nature of the particles. The track length is, in principle, simply related to atomic number, but it has proven difficult to apply in practice [105,106]. Measurement of the track etch rate has been more useful and indicates that there appears to be no sharp threshold ionization value. Tracks from light ions ($Z < 18$) etch more slowly than those from heavier ions, and they are more readily erased by thermal annealing [105, 106].

The interpretation of nuclear track data is model dependent "due to erosion of grains by impact and sputtering, or to fading of the tracks over long intervals of time" [107]. This erosion is of the order of one angstrom per year, by sputtering, and one millimeter per million years by micrometeorite impact. Thus, only those surfaces that escape the sputtering and erosion processes yield meaningful data about exposure ages. The intensity of the irradiation is shown by these few uneroded surfaces. A millimeter-sized crystal at the bottom of a vug from an Apollo 15 rock [108], estimated to have been uncovered and exposed about 2×10^4 years ago, has a track density of 5×10^{10} tracks/cm² on its surface, and some soil grains that have escaped sputtering have surface track densities of 10^{11} /cm². Unshielded rock and grain surfaces have track densities typically about 10^8 tracks/cm². Because of experimental difficulties, the error in track counts from different investigators is on the order of $\pm 20\%$ [105].

~~The cosmic ray produced tracks need to be distinguished from fission tracks due to ²³⁸U and to ²⁴⁴Pu. High uranium concentrations can contribute more than 10^8 fission tracks/cm² at grain boundaries or in inclusions. Their non-uniform distribution, differing etch pit characteristics, and the low fission track density in common minerals (where uranium is low in abundance) enable them to be distinguished from the cosmic ray tracks. Tracks due to the spontaneous fission of ²³⁸U are commonly observed, but those from ²⁴⁴Pu (half-life of 82×10^6 yr.) are difficult to find in lunar rocks. Most of the mare basalts are too young to contain measurable amounts of decay products. A slightly more favorable environment exists in uranium-rich mineral phases in the older lunar rocks. Tracks due to ²⁴⁴Pu fission occur in a whitlockite crystal from the Fra Mauro breccias (14321) [109]. This sample was heavily shielded from cosmic rays until about 25 million years ago.~~

~~The possible existence of superheavy elements has been much debated. The principal evidence adduced was the presence of long fission tracks. These >20 micron tracks, which were identified as being due to extinct superheavy elements, are probably "fresh" tracks due to cosmic ray nuclei. There is no~~

pages 159 – 164 deleted

lunar chronology. A very full discussion of the problems of interpretation of the irradiation record in this context is given by Burnett and Woolum [137].

4.10.1 Nuclear Track Data

Much information on exposure ages and regolith history has been obtained from the track studies. Track production at shallow depths (< 0.5 cm) is dominated by solar flares, while at greater depths, galactic cosmic ray tracks predominate [105, 106]. The “sun tan” exposure time is defined as the period during which a rock was at the surface of the Moon (usually less than 3 million years), while the “sub-decimeter” exposure time is the period during which a rock was within 10 cm of the surface (typically 1–100 million years).

High track densities, indicating surface exposure, are found throughout the core samples. The early interpretations were of a high rate of regolith turnover, but it quickly became clear that the regolith was stratified, and models involving deposition of thin layers, stirring of the surface, and burial by subsequent layers were adopted and so “throwout” models became preferred to “gardening” models [138]. This became clear from the study of the Apollo 15 deep core which contained forty-two strata, in which high track densities were distributed throughout the 242-cm core length and were independent of depth.

Many micron-sized particles with very high track densities have an amorphous surface layer from the solar bombardment. Each layer in the core contains grains throughout that were once at the “very surface,” indicating good mixing of each layer before burial. Stirring takes place to a depth of a few centimeters. Deeper stirring is rare. Instead, overturning of layers by cratering occurs. Surface layers seem to survive for periods of from 1 to 50 million years before burial, as indicated by cratering studies (Section 4.3.2).

Exposure ages of rocks lying on the surface have been measured (Table 4.10). Most (80%) have a complex exposure history. Erosion by the micro-meteorite bombardment and solar wind sputtering exposes fresh surfaces at rates of about one millimeter per million years.

Information about the exposure of old highland breccia fragments may be obtained from the track data, but this is offset by annealing due to heating during breccia formation. Because of this, the use of mare basalt rocks or individual grains in the regolith is preferred in cosmic ray studies. The tracks are largely inherited from the original parent materials which must have had exposure at the very top surface. Grains with track densities of $\geq 10^8/\text{cm}^2$ occur within the breccia matrix. The track densities correlate with metamorphic grade. Low track counts due to thermal annealing have occurred [139]. Tracks are absent in the well-recrystallized breccias (e.g., 15418, 61016, 66055, 67015) [140]. Tracks vanish first from the glasses during annealing, then

Table 4.10 Surface residence times for rocks apparently exposed in one orientation.

Rock	Mass (g)	Surface Residence Time (m.y.)
12018	787	1.7
12038	746	1.3
12022	1864	~10
62295	251	2.7
74275	1493	2.8
67915	*	50 [†]
68815	*	2 [†]
76315	*	21 [†]

* Boulder chip.

[†] Surface residence time = total cosmic ray exposure time.

From Burnett, D. S., and Woolum, D. S. (1977) *PCE* 10: 87.

generally from olivine, pyroxenes, and feldspar in that order with increasing temperature.

There are a number of similarities between the lunar breccias and the gas-rich meteorites (e.g., Kapoeta, Fayetteville), which also contain grains exposed before incorporation in the meteorite with track densities of $\geq 10^{10}/\text{cm}^2$. Preserved solar flare tracks are seen even in the most recrystallized chondrites (e.g., LL6 grade [140, 141]), suggesting that even the most metamorphosed chondritic meteorites correspond only to the less metamorphosed lunar breccias [142]. The data seem consistent with the formation of the gas-rich meteorites in a regolith-type environment less extreme than that of the lunar surface, possibly on asteroid surfaces [140]. In this context, observations of the asteroid Toro suggest that it has a lunar-type regolith [143].

4.10.2 Rare Gas Data

The exposure history of the regolith and of surface rocks was one of the first applications of the rare gas studies. Of the various age methods, the most reliable are ^{81}Kr - ^{83}Kr , ^{21}Ne , and ^{38}Ar ages [144]. The ^3He ages are subject to loss of He by diffusion. A full review of the data is provided by Burnett and Woolum [137] with appropriate cautionary tales.

The impact events dated by the ^{81}Kr technique are given in Table 4.11. The dating, of course, depends on the proper sampling of the ejecta blanket. Much confusion arose over the age of South Ray (Apollo 16), one of the freshest craters on the lunar surface. The ages of about 2 million years quoted in Table 4.11 are from rocks, and are in accord with the geological criteria [146]. Many of the soils, interpreted as South Ray ejecta, are far removed from the crater rim. South Ray is 640 m in diameter. The astronaut traverses came no closer than about 3 km, and fine ejecta from South Ray at about five

pages 168 – 170 deleted

4.14 Organic Geochemistry and Exobiology

A complete account of the organic geochemistry investigations on lunar samples was given previously [174]. Little further work has been done on this subject and the interested reader is referred to the previous summary.

The account of the search for life in the lunar samples is given in the same reference [174] and need not be repeated here. It should be noted that the absence of life on the Moon was in accordance with the prediction of C. Huyghens in 1757 that "the Moon has no air or atmosphere surrounding it as we have, [and I] cannot imagine how any plants or animals whose whole nourishment comes from fluid bodies, can thrive in a dry, waterless, parched soil" [175]. The search for life on Mars has been dealt with exhaustively in other references [176, 177] and will not be treated here. The effective absence of organic compounds at the parts per billion level in the Viking organic mass spectrometric experiment seems decisive [178]. This contrasts with the development of life on Earth [179].

References and Notes

1. Hood, L. L., and Schubert, G. (1980) *Science*. 208: 49.
2. Thompson, T. W., et al. (1974) *Moon*. 10: 87; (1981) *Icarus*. 46: 201; See also Pettengill, G. H. (1978) *Ann. Rev. Astron. Astrophys.* 16: 265 for an extended review of radar observations of planets and satellites. See also Schultz, P. H., and Mendell, W. (1978) *PLC* 9: 2857 for a discussion of orbital infrared observations.
3. Keihm, S. J., et al. (1973) *EPSL*. 19: 337; (1973) *PLC* 4: 2503; Strangway, D. W., and Olhoeft, G. R. (1977) *Phil. Trans. Roy. Soc.* A285: 441.
4. Olhoeft, G. R., et al. (1975) *PLC* 6: 3333.
5. See Tang, C. H., et al. (1977) *JGR*. 82: 4305 for surface electrical properties of Mars.
6. See Hess, S. L., et al. (1977) *JGR*. 82: 4559 for a description of Martian meteorology.
7. See Moore, H. J., et al. (1977) *JGR*. 82: 4497 for a description of Martian surface properties.
8. Saari, J. M. (1964) *Icarus*. 3: 161.
9. Mendell, W. W., and Low, F. J. (1970) *JGR*. 75: 3319.
10. Gold, T. (1971) *PLC* 2: 2675.
11. The extreme case is the presence of the layer of "light gray fines" (12033) at Apollo 12, a KREEP-rich layer of exotic origin.
12. The XRF experiment samples only the top few microns of the surface. The gamma-ray experiment looks somewhat deeper (10–20 cm). Adler, I., et al. (1973) *PLC* 4: 2783; Metzger, A. E., et al. (1973) *Science*. 179: 800.
13. McCoy, J. E., and Criswell, D. R. (1974) *PLC* 5: 2991.
14. Berg, O. E. (1978) *EPSL*. 39: 377.
15. Hörz, F. (1973) NASA SP 315, 7–24.
16. Gold, T. (1970) *Icarus*. 12: 360; (1971) *Apollo 14 PSR*, p. 239.
17. A major source of information on the lunar regolith is given in *The Moon* (1975), Vol. 13, p. 1–359, which contains the proceedings of a conference on the lunar regolith held

- at the Lunar Science Institute, Houston, Texas, November 1974. See also an excellent review by Langevin, Y., and Arnold, J. R., (1977) *Ann. Rev. Earth Planet. Sci.* 5: 499. See also Regolith Conference Abstracts, LPI. Nov. 1981.
18. NASA SP 289 (1972) 5-23.
 19. Cooper, M. R., et al. (1974) *Rev. Geophys. Space Phys.* 12: 291.
 20. Peeples, W. J., et al. (1978) *JGR*. 83: 3459.
 21. Freeman, F. J. (1981) USGS Prof. Paper 1048, Chap. F.
 22. Eberhardt, P. (1973) *Moon*. 8: 104.
 23. Houston, W. N., et al. (1974) *PLC* 5: 2361; Carrier, W. D., et al. (1973) *PLC* 3: 3213; Houston, W. N., et al., *ibid.*, 3255; Mitchell, J. K., et al., *ibid.*, 3235; Mitchell, J. K., et al. (1973) *PLC* 4: 2437.
 24. Cherkasov, I. I., and Shvarev, V. V. (1975) *Lunar Soil Science* (Trans. N. Kaner), Keter Publishing House, Jerusalem, 170 pp.
 25. Quaide, W., and Oberbeck, V. (1975) *Moon*. 13: 27.
 26. Hörz, F. (1977) *PCE* 10: 3.
 27. Nishiizumi, K., et al. (1979) *EPSL*. 44: 409.
 28. Schmitt, R. A., and Laul, J. C. (1973) *Moon*. 8: 190.
 29. Schonfeld, E., and Meyer, C. (1972) *PLC* 3: 1415.
 30. Shoemaker, E. M., et al. (1971) *PLC* 1: 2399.
 31. Wood, J. A., et al. (1970) *PLC* 1: 965.
 32. Bhandari, N., et al. (1972) *PLC* 3: 2811.
 33. Papanastassiou, D. A., and Wasserburg, G. J. (1970) *EPSL*. 8: 1, 269; (1971) *EPSL*. 11: 37, 12: 36; (1972) *EPSL*. 13: 368; 17: 52.
 34. Cliff, R. A., et al. (1972) *JGR*. 77: 2007; Mark, R. K., et al. (1973) *PLC* 4: 1785; Murthy, V. R., et al. (1972) *PLC* 3: 1503.
 35. Wetherill, G. W. (1971) *Science*. 173: 389.
 36. The $^{87}\text{Sr}/^{86}\text{Sr}$ ratio of 0.69898 is the Basaltic Achondrite Best Initial (or BABI) ratio [33].
 37. Nyquist, L. E., et al. (1973) *PLC* 4: 1839.
 38. Schaal, R. B., and Hörz, F. (1980) *PLC* 11: 1679.
 39. McKay, D. A., et al. (1970) *PLC* 1: 673.
 40. Chao, E. C. T., et al. (1971) *JGR*. 75: 7445.
 41. McKay, D. S., et al. (1972) *PLC* 3: 988.
 42. McKay, D. S., et al. (1971) *PLC* 2: 755.
 43. Taylor, G. J., et al. (1978) *PLC* 9: 1959.
 44. Adams, J. B., and McCord, T. B. (1973) *PLC* 4: 163; Rhodes, J. M., et al. (1975) *PLC* 6: 2291.
 45. Via, W. N., and Taylor, L. A. (1976) *PLC* 7: 393.
 46. Papike, J. J. (1981) LPS XII: 805.
 47. Stroube, W. B., et al. (1978) *Meteoritics*. 13: 201.
 48. Taylor, S. R., and McLennan, S. M. (1979) *GCA*. 43: 1551.
 49. Simonds, C. H., et al. (1978) *JGR*. 83: 2773.
 50. Gooding, J. L., et al. (1980) *EPSL*. 50: 171.
 51. Gooding, J. L., and Keil, K. (1981) *Meteoritics*. 16: 17.
 52. Cloud, P. (1970) *PLC* 1: 1794.
 53. Taylor, S. R. (1973) *Earth Sci. Rev.* 9: 101.
 54. Roedder, E., and Weiblen, P. W. (1970) *PLC* 1: 801.
 55. Glass, B. P. (1976) *PLC* 7: 679.
 56. Glass, B. P., and Barlow, R. A. (1979) *Meteoritics*. 14: 55.
 57. Mason, B. H. (1979) *Smith. Contrib. Earth Sci.* 22: 14.
 58. Glass, B. P. (1972) *JGR*. 77: 7057; Frey, F. A. (1977) *EPSL*. 35: 43.

59. Shaw, H. F., and Wasserburg, G. J. (1981) LPS XII: 967.
60. Taylor, H. P., and Epstein, S. (1970) *PLC 1*: 613.
61. Schnetzler, C. C. (1970) *Meteoritics*. 5: 221.
62. O'Keefe, J. A. (1970) *Science*. 168: 1209.
63. Epstein, S., and Taylor, H. P. (1973) *PLC 4*: 1559.
64. Kozyrev, N. (1963) *Nature*. 198: 979.
65. Pike, R. J. (1980) USGS Prof. Paper 1046 C.
66. Chao, E. C. T., et al. (1962) *Science*. 135: 97; (1964) *GCA*. 28: 971.
67. Labotka, T. C., et al. (1980) *PLC 11*: 1285.
68. Laul, J. C., and Papike, J. J. (1980) *PLC 11*: 1307.
69. Rhodes, J. M. (1977) *Phil. Trans. Roy. Soc.* A285: 293.
70. Hörz, F. (1978) *PLC 9*: 3311.
71. Hubbard, N. J. (1979) *PLC 10*: 1753.
72. Laul, L. C., and Papike, J. J. (1980) *PLC 11*: 1307. It should be noted that both Ni and Co data reported in this study are probably contaminated through the use of rhodium plated nickel sieves.
73. Korotev, R. L., et al. (1980) *PLC 11*: 395.
74. Muehlberger, W. R., et al. (1980) *Lunar Highlands Crust*, p. 1.
75. Kempa, M. J., et al. (1980) *PLC 11*: 1341.
76. Heiken, G. (1975) *Rev. Geophys. Space Phys.* 13: 567.
77. Nagata, T., et al. (1974) *PLC 5*: 2815.
78. Cisowski, C. S., et al. (1974) *PLC 5*: 2841.
79. Chou, C. L., and Pearce, G. W. (1976) *PLC 7*: 779.
80. Morris, R. V. (1980) *PLC 11*: 1697.
81. Boynton, W. V., et al. (1976) *EPSL*. 29: 21.
82. Wëgmuller, F., et al. (1980) *PLC 11*: 1763.
83. Butler, P. (1978) *PLC 9*: 1459.
84. Cirlin, E. H., et al. (1978) *PLC 9*: 2049.
85. Cirlin, E. H., and Housley, R. M. (1979) *PLC 10*: 341; (1981) *PLC 12*: 529.
86. Gibson, E. K. (1977) *PCE 10*: 57.
87. Kurat, G., and Keil, K. (1972) *EPSL*. 14: 7.
88. Arnold, J. R. (1979) *JGR*. 84: 5659.
89. Fremlin, J. H. (1979) *Nature*. 278: 598.
90. Morgan, J. W., et al. (1977) NASA SP 370, 659.
91. Wasson, J. T., et al. (1975) *Moon*. 13: 121.
92. Schneider, E. (1973) *PLC 4*: 3277.
93. Hörz, F., et al. (1971) *JGR*. 76: 5770; Hartung, J. B., et al. (1973) *PLC 4*: 3213; Morrison, D. A., et al., *ibid.*, 3235; Neukum, G., et al., *ibid.*, 3255; Schneider, E., et al., *ibid.*, 3277; Morrison, D. A., et al. (1972) *PLC 3*: 2767; Neukum, G., et al., *ibid.*, 2793; Gault, D. E., et al., *ibid.*, 2713; Hartung, J., et al., *ibid.*, 2735; Hörz, F. (1975) *Planet. Space Sci.* 23: 151.
94. Frondel, C., et al. (1970) *PLC 1*: 445; Fredriksson, K., et al., *ibid.*, 419.
95. Brownlee, D. E., et al. (1977) *PLC 8*: 149.
96. Hörz, F., et al. (1975) *PLC 5*: 2397.
97. Duennebier, F. K. (1976) *Science*. 192: 1000.
98. Borg, J. (1980) *Ancient Sun*, p. 431.
99. Pepin, R. O. (1980) *Ancient Sun*, p. 411.
100. Marti, K. (1980) *Ancient Sun*, p. 423.
101. Walker, R. M. (1975) *Ann. Rev. Earth Planet. Sci.* 3: 99.
102. Crozaz, G. (1977) *PCE 10*: 197.
103. Crozaz, G. (1980) *Ancient Sun*, p. 331.

104. Macdougall, J. D., et al. (1974) *Science*. 183: 73.
105. Price, R. B., Fleisher, R. L., and Walker, R. M. (1975) *Nuclear Tracks*, Univ. Calif. Press.
106. Lal, D. (1972) *Space Sci. Rev.* 14: 45.
107. Herrman, G. (1979) *Nature*. 280: 543.
108. Phakey, P. P., et al. (1972) *PLC* 3: 2905.
109. Crozaz, G., et al. (1972) *PLC* 3: 1623.
110. Crozaz, G. (1980) *Ancient Sun*, p. 311.
111. Epstein, S., and Taylor, H. P. (1970) *PLC* 1: 1085.
112. Eglinton, G., et al. (1974) *Topics in Current Chemistry*. 44: 88.
113. Pillinger, C. T. (1979) *PCE* 11: 61.
114. Becker, R. H., and Clayton, R. N. (1975) *PLC* 6: 2131.
115. Becker, R. H., et al. (1977) *PLC* 8: 3685.
116. Gibson, E. K. (1977) *PCE* 10: 57.
117. Muller, O. (1979) *PCE* 11: 47.
118. Clayton, R. N., and Thiemens, N. H. (1980) *Ancient Sun*, p. 463.
119. Kerridge, J. F. (1980) *Ancient Sun*, p. 475.
120. Goel, P. S., et al. (1975) *GCA*. 39: 1347.
121. Kerridge, J. F., et al. (1975) *PLC* 6: 2151.
122. Thode, H. G., and Rees, C. E. (1979) *PLC* 10: 1629.
123. Heymann, D. (1977) *PCE* 10: 45.
124. Heymann, D., and Yaniv, A. (1970) *PLC* 1: 1261.
125. Eberhardt, P., et al. (1970) *PLC* 1: 1037.
126. Baur, H., et al. (1972) *PLC* 3: 1947.
127. Signer, P., et al. (1977) *Phil. Trans. Roy. Soc.* A285: 385.
128. Yaniv, A., and Heymann, D. (1972) *PLC* 3: 1967.
129. Schultz, L. (1979) *PCE* 11: 39.
130. McElroy, M. B., and Prather, M. J. (1981) *Nature*. 293: 535. This article contains a review of the noble gases in the terrestrial planets.
131. Reedy, R. C. (1980) *Ancient Sun*, p. 370.
132. Wahlen, M., et al. (1972) *PLC* 3: 1719.
133. Reedy, R. C., and Arnold, J. R. (1972) *JGR*. 77: 537.
134. Fields, P. R., et al. (1973) *PLC* 4: 2123.
135. Burnett, D. S., and Woolum, D. S. (1974) *PLC* 5: 2061.
136. Russ, G. P. (1973) *EPSL*. 16: 275.
137. Burnett, D. S., and Woolum, D. S. (1977) *PCE* 10: 63.
138. Arrhenius, G., et al. (1971) *PLC* 2: 2583.
139. Hart, H. R., et al. (1972) *PLC* 3: 2831; Hutcheon, I. D., et al., *ibid.*, 2845, 2863; Dran, J. C., et al. (1972) *PLC* 3: 2883; Yuhas, D. E., et al. (1972) *PLC* 3: 2941.
140. Macdougall, J. D., et al. (1973) *PLC* 4: 2319.
141. Van Schmus, W. R., and Wood, J. A. (1967) *GCA*. 31: 747.
142. Crozaz, G., et al. (1974) *PLC* 5: 2475.
143. Dunlap, J. L., et al. (1973) *Astron. J.* 78: 491.
144. Marti, K. (1967) *Phys. Rev. Lett.* 18: 264; Lugmair, G. W., and Marti, K. (1972) *PLC* 3: 1891; Marti, K., et al. (1973) *PLC* 4: 2037.
145. Kirsten, T., et al. (1972) *PLC* 3: 1865.
146. McKay, D. S., and Heiken, G. H. (1973) *PLC* 4: 41.
147. Drozd, R. J., et al. (1977) *PLC* 8: 3027.
148. Lucchitta, B. K. (1979) *Icarus*. 37: 46.
149. *The Ancient Sun: Fossil Record in the Earth, Moon and Meteorites* (1980) (eds., Pepin, R. O., et al.), Pergamon, 581 pp.

150. Those readers with a historical bent will reflect on the curious fact that the Maunder Minimum of solar activity 1645–1715, coincided with the life of the Sun King (Louis XIV, 1638–1715), a correlation no doubt of use to Francophiles and Francophobes alike.
151. Stuiver, M., and Grootes, P. M. (1980) *Ancient Sun*, p. 165.
152. Fairhill, A. W., and Yorg, I. C. (1980) *Ancient Sun*, p. 175.
153. Raisbeck, G. M., and Yiou, F. (1980) *Ancient Sun*, p. 185.
154. Zinner, E. (1980) *Ancient Sun*, p. 201.
155. Zook, H. A. (1980) *Ancient Sun*, p. 245.
156. Macdougall, J. D., and Kothari, B. K. (1976) *EPSL*. 33: 36.
157. Goswami, J. N. (1980) *Ancient Sun*, p. 347.
158. Crozaz, G., and Walker, R. M. (1971) *Science*. 171: 1237.
159. Marti, K. (1980) *Ancient Sun*, p. 423.
160. Windley, B. F. (1977) *The Evolving Continents*, Wiley.
161. Newkirk, G. (1980) *Ancient Sun*, p. 293.
162. NASA SP-330.
163. Hodges, R. R., et al. (1973) *PLC 4*: 2854; (1974) *Icarus*. 21: 415.
164. Hoffman, J. H., et al. (1973) *PLC 4*: 2865.
165. Hodges, R. R., et al. (1974) *Icarus*. 21: 415 gives a comprehensive review of the lunar atmosphere.
166. Chernyak, Y. B. (1978) *Nature*. 273: 497.
167. McElroy, M. B., et al. (1977) *JGR*. 82: 4379.
168. Hoffman, J. H., et al. (1980) *JGR*. 85: 7882.
169. Donahue, T. M., et al. (1981) *GRL*. In press.
170. Anders, E., and Owen, T. (1977) *Science*. 198: 453.
171. Pollack, J. B., and Black, D. C. (1979) *Science*. 205: 56; Pollack, J. B., and Yung, Y. L. (1980) *Ann Rev. Earth Planet. Sci.* 8: 425.
172. Wetherill, G. W. (1981) *Icarus*. In press.
173. Hostetler, C. J. (1981) *PLC 12*: 1387.
174. Taylor, S. R. (1975) *Lunar Science: A Post-Apollo View*, Pergamon, N.Y., p. 110–114.
175. Huyghens, C. (1757) *Cosmotheoros*.
176. The biological experiments are described in (1977) *JGR*. 82: 4659–4677.
177. An extended and readable account is given by H. S. F. Cooper (1980) in *The Search for Life on Mars*, Dial Books.
178. Biemann, K., et al. (1977) *JGR*. 82: 4641.
179. Schopf, J. W., ed. (1982) *Origin and Evolution of the Earth's Earliest Biosphere*, Princeton Univ. Press.